

1 **Orientating the future bio-macromolecular electron microscopy**

2 Fei Sun^{1,2,3}

3 ¹ Center for biological imaging, Institute of Biophysics, Chinese Academy of Sciences;

4 ² Center for Excellent, National Laboratory of Biomacromolecule, Institute of Biophysics,
5 Chinese Academy of Sciences; Datun Road 15, Chaoyang District, Beijing 100101, China.

6 ³ School of Life Science, University of Chinese Academy of Sciences.

7 Email: feisun@ibp.ac.cn

8

9

1 **ABSTRACT**

2 With forty years of developments, bio-macromolecule cryo-electron microscopy has
3 met its revolution of resolution and is playing a very important role in structural biology
4 study. According to different specimen states, cryo-electron microscopy (cryo-EM) involves
5 three specific techniques, single particle analysis (SPA), electron tomography and sub-
6 tomogram averaging, and electron diffraction. All these three techniques have not realized
7 their full potentials of solving structures of bio-macromolecules and therefore need to be
8 developed in the future. In this review, the current existing bottlenecks of cryo-EM SPA are
9 discussed with theoretical analysis, which includes air-water interface during specimen
10 cryo-vitrification, bio-macromolecular conformational heterogeneity, focus gradient within
11 thick specimen, and electron radiation damage. Besides, potential solutions of these
12 bottlenecks are proposed and discussed, which are worthy of further investigations in the
13 future.

14 **KEYWORDS**

15 Cryo-electron microscopy; Air-water interface; Conformational heterogeneity; Focus
16 gradient; Radiation damage.

17

18

1 **1. Introduction**

2 Revealing the detailed 3D structure of bio-macromolecules is one of the important steps
3 to understand the life. In recent years, cryo-electron microscopy (cryo-EM) has completed
4 its revolution and been becoming one of the major biophysical techniques to study the 3D
5 structures of bio-macromolecules, especially of membrane protein complexes and supra
6 macromolecular assemblies, giving a big impact on our understanding of the life.

7 The development of cryo-EM technology started from the last century in 70~80s when
8 the significant electron radiation damage of biological specimen was discovered and the
9 low-dose illumination technique was proposed [18, 34], the cryo-vitrification method to fix
10 the native structure of biological specimen was established [1, 79], and the image analysis
11 theory to process the low signal-to-noise-ratio (SNR) low-dose cryo-EM micrographs of
12 bio-macromolecules was developed [24]. The potential of electron microscopy to
13 determine the high resolution structure of bio-macromolecules had been revealed by the
14 3D structure of purple membrane in 1975 [37] and seriously discussed with a theoretical
15 consideration in 1995 [35]. In recent years, with the instrumental advances in electron
16 optics and improved stabilities of electron microscopes, the development of sophisticated
17 image processing software [33, 59, 68] and the automation of data collection [6, 52, 78],
18 the improvement of phase plate technology [43, 44], especially the success of the direct
19 electron detector [3, 48, 49], cryo-EM technology has reached its revolution in resolution
20 [45] with the milestone work that the structure of transient receptor potential cation channel
21 TRPV1 was determined to 3.4 angstrom in 2013 [49] and the structure of the glutamate

1 dehydrogenase (GDH) was solved to atomic level in 2016 [55] by cryo-EM. More and more
2 supra bio-macromolecular structures, e.g. spliceosome [87], photosynthetic complex [85],
3 and mitochondrial respiratory complex [83], have been solved to near atomic level, which
4 could not be achieved by using traditional structural biology approaches.

5 According to the states of the biological specimen and the experimental workflow, cryo-
6 EM technologies can be classified into three different techniques, cryo-EM single particle
7 analysis (SPA), cryo-electron tomography (cryo-ET) and sub-tomogram analysis (STA),
8 and cryo-electron diffraction (cryo-ED). Cryo-EM SPA is used to analyze the 3D structure
9 of purified bio-macromolecules in solution, which are cryo-vitrified into a thin ice layer. Ten
10 thousands of cryo-EM images of the bio-macromolecule are needed to increase SNR and
11 reconstruct a high resolution structure [62]. Cryo-ET can reconstruct the native 3D structure
12 of a local region within a cell or tissue and the *in situ* structure of bio-macromolecules can
13 be further analyzed by STA [7]. There is no need to purify bio-macromolecules from cell or
14 tissue while hundreds of tomograms of cryo-lamella of cell or tissue are needed to obtain
15 a high resolution *in situ* structure of bio-macromolecules. Cryo-ED is a kind of technique to
16 use cryo-electron microscope to analyze the crystallized biological specimen. It collects
17 the electron diffraction data from 2D crystals or 3D nano-crystals of bio-macromolecules
18 and then solves the high resolution structures using crystallographic theories, where the
19 technique to study 2D crystals was used to be called electron crystallography [31] and the
20 one to study 3D nano-crystals emerged recently and was called as micro-electron
21 diffraction [74]

1 Cryo-EM SPA has been developed mature enough in past decades and been becoming
2 the major approach in the current structural biology study. The Nobel prize in chemistry in
3 2017 was also given to Jacques Dubochet, Joachim Frank and Richard Henderson for their
4 great dedicative work in developing cryo-EM SPA technique. Cryo-ET STA has been also
5 developed quickly in recent years and will become an important also a unique approach to
6 study the *in situ* structure of bio-macromolecules in the future. In this paper, I will discuss
7 the current bottlenecks of cryo-EM SPA and present some potential solutions in my
8 personal view.

9 **2. Current technical bottlenecks in cryo-EM SPA**

10 There have been many good reviews to describe the technique of cryo-EM SPA
11 including the theory, workflow, image processing and applications [14, 57, 80]. In brief,
12 cryo-EM SPA starts from the cryo-vitrification of bio-macromolecular solution and needs to
13 collect thousands of high quality cryo-EM micrographs in a high-throughput way with a
14 limited illumination dose ($20 \sim 60 \text{ e}/\text{\AA}^2$ normally), a defined magnification yielding a proper
15 pixel size ($0.8 \sim 1.5 \text{ \AA}/\text{pixel}$ normally), and a proper defocus range ($0.8 \sim 3.0 \text{ }\mu\text{m}$). The
16 subsequent image processing includes micrograph correction (motion and distortion
17 correction, dose weighting) and evaluation, contrast transfer function estimation, particle
18 picking and sorting, 2D and 3D classification, orientation refinement and reconstruction,
19 and post-processing (map sharpening). Since the limited illumination dose yields a very
20 noisy raw image of bio-macromolecules that are embedded in vitreous ice, ten thousands
21 of particle images are needed to increase SNR. Thus, the basic assumption behind cryo-

1 EM SPA is that all the analyzed bio-macromolecules should have an identical structure and
2 conformation, which is actually not always true.

3 Starting from 2013 when the near atomic structure of TRPV1 was first solved [49], the
4 number of bio-macromolecular structures studied by cryo-EM SPA increased quickly. Till
5 2017, there are already 5541 cryo-EM maps deposited in electron microscopy database
6 (EMDB, <http://www.ebi.ac.uk/pdbe/emdb>) [58] while there are only 1566 entries in 2012.
7 Most of the deposited maps were obtained by cryo-EM SPA. However, only a small portion
8 of the map (313/5541) can reach a resolution higher than 4 Å and only a few structures
9 can be solved to the resolution higher than 3 Å (**Figure 1**), which actually forms a barrier
10 for cryo-EM SPA to be widely applied into pharmaceutical industry.

11 Several bottlenecks are still there in cryo-EM SPA from sample preparation, data
12 collection to image processing, which forms the barrier to reach a better resolution. In cryo-
13 vitrification during sample preparation, the existence of air-water interface increases the
14 possibility of disassociation and denature of bio-macromolecules, which prohibited many
15 fragile macromolecular complexes to be studied by cryo-EM SPA. The existence of intrinsic
16 conformational flexibility of bio-macromolecules rule out the basic assumption upon the
17 identical structure and conformation in cryo-EM SPA, which restricted approaching high
18 resolution. During cryo-EM imaging, the SNR from the current instrument and hardware is
19 still not enough to study the high resolution 3D structures of bio-macromolecules when
20 their molecular weight is smaller than 60 kDa. The phase plate and direct dection detector
21 technologies can be improved better to increase the current cryo-EM SNR. The cryo-

1 electron microscope can be made more stable, easy to use and dedicative for the cryo-EM
2 SPA workflow with much improved throughput. When the size of bio-macromolecule
3 becomes large or the thickness of biological material increases, the existence of the Ewald
4 sphere effect and focus gradient will limit the approachable resolution of cryo-EM imaging
5 in the current theoretical framework, which needs to be solved in both experimental and
6 image processing procedures. The ultimate bottleneck of cryo-EM SPA is the physical
7 nature of radiation damage of bio-macromolecules during cryo-EM imaging, which can not
8 be avoided and is the key limitation of achieving atomic resolution in cryo-EM SPA.

9 Glaeser has made a very good discussion of the above bottlenecks and given
10 thoughtful perspectives [27]. Here, I would like to focus on cryo-vitrification, conformational
11 heterogeneity, thick sample, and electron radiation damage, further discuss these
12 limitations in theory, and propose new solutions to solve these bottlenecks.

13 **2.1 Cryo-vitrification and air-water interface**

14 The current cryo-vitrification method was originally invented by Dubochet's group in
15 1984 [1], which is called plunge freezing. The EM grid coated with a carbon supporting film
16 is pre-treated with plasma cleaner and then nipped by a fine tweezer and mounted onto
17 the plunge freezer. 3~5 μ l bio-macromolecule solution is dropped onto the supporting film.
18 After a few seconds of incubation, most of the liquid is blotted with filter paper, leaving a
19 thin layer of the solution (30 ~ 50 nm thickness) on the grid. Subsequently, the grid is then
20 quickly plunged into liquid ethane that is pre-cooled by liquid nitrogen, resulting the
21 vitrification of the thin solution layer. Finally, the bio-macromolecules are embedded in the

1 vitreous ice with their native structure preserved. The procedure of this cryo-vitrification
2 method did not change much since its invention and is still now widely used in the world
3 for cryo-EM SPA. Several vendors made commercialized instruments (Thermo Fisher
4 Vitrobot, Leica EM GP and Gatan CP3) for cryo-vitrification, which increase the throughput
5 and reproducibility by controlling experimental parameters (e.g. humidity, temperature,
6 blotting time) accurately.

7 However, more and more labs found that the homogeneity of the bio-macromolecule
8 became significantly decreased from cryo-vitrified sample when compared with the
9 negatively stained sample. The worst case is that although the specimen shows even
10 distribution with homogenous size and shape from the negative stain electron micrographs,
11 few particles could be identified/recognized from the cryo-EM micrographs (**Figure 2A**).
12 The reason of this phenomena has been fully discussed by Glaeser and colleagues [28,
13 29] and now widely recognized to be the effect from the air-water interface (**Figure 2B**).

14 During plunge freezing, the thin solution layer after filter paper blotting results a very
15 large surface-to-volume ratio ($\sim 20 \text{ um}^{-1}$) in comparison with its original value of ($\sim 2.0 \text{ e-3}$
16 um^{-1}). Thus the bio-macromolecule in the thin layer of the solution has large opportunity to
17 reach the surface. The movement of the bio-macromolecule $\sqrt{x^2}$ follows the Brownian
18 motion law according to the following equation,

$$19 \quad \frac{x^2}{t} = \frac{k_B T}{3\pi\eta r} \quad (1)$$

20 where, t is the time of the motion, r is the radius of the bio-macromolecule, η is the

1 coefficient of viscosity of the solution (for water at 10°C, it is 1.308 mPa.s), k_B is the
 2 Boltzmann constant, and T is the temperature in Kelvin. For the thickness of 50 nm of the
 3 layer and a 20 nm diameter of the bio-macromolecule, the averaged time (at $T = 283$ K)
 4 for the bio-macromolecule reaching the surface can be estimated as ~ 20 ms. The time
 5 can be even shorter (~ 6 ms) for a thinner ice (40 nm thickness) and smaller bio-
 6 macromolecule (10 nm diameter). As a result, upon the formation of the thin layer of the
 7 solution, the bio-macromolecules can quickly approach the surface called the air-water
 8 interface, which has the large possibility to induce denaturation of the bio-macromolecule
 9 [28]. The thermodynamics of this procedure can be further described as below (**Figure 2B**),



11 where A_V represents the concentration of bio-macromolecule in the solution, A_S
 12 represents the concentration of bio-macromolecule bound to the air water interface, and
 13 A_D represents the concentration of denatured bio-macromolecule. Thus, the speed of bio-
 14 macromolecule denaturation is determined by the reaction constants k_1 , k_2 , and k_3 . If the
 15 order of k_3 can be estimated of $1 \times 10^6 s^{-1}$, the denaturation of the bio-macromolecule
 16 can occur within 1 μs .

17 During plunge freezing, the time normally takes seconds from the completion of blotting
 18 to plunging into liquid ethane, which are much longer than the one for bio-macromolecules
 19 approaching to the air-water interface and denatured. Therefore, it can be explained why
 20 it was difficult to obtain good cryo-EM micrographs for those fragile bio-macromolecules

1 that are easily denatured (or disassociated) although they can be well captured in negative
2 stain electron micrographs (**Figure 2A**).

3 The existence of air-water interface has become one of the most important bottlenecks
4 for cryo-EM SPA to obtain high resolution structures of many bio-macromolecules. To
5 overcome this bottleneck, people have developed multiple ways to reduce the air-water
6 interface by utilizing an additional ultrathin ($\sim 2\text{nm}$) carbon film [28] or developing affinity
7 grids [42, 90]. Adding surfactant into the solution could be also useful to form a 'cover-slip'
8 at the air-water interface and therefore protect the bio-macromolecules from denaturation
9 [60]. In addition, the new instruments using automatic robotics have been recently
10 developed, e.g. Spotiton [61] and 'grid writer' [2], which avoid paper blotting and can
11 minimize the time between the formation of thin layer and the plunge freezing to $\sim 50\text{ ms}$,
12 which therefore greatly reduce the possibility of the molecule approaching to the surface.

13 According to the equations (1) and (2), there are also other ways to reduce the effect
14 of air-water interface. Using a high concentration of bio-macromolecules during vitrification
15 may increase the coefficient of viscosity and thus increase the time of approaching to the
16 surface. Meanwhile, the high concentration can also have a chance to saturate the air-
17 water interface with the denatured molecules and thus allow enough number of native
18 molecules left in the solution. To be noted that, the high concentration could increase the
19 difficulty in the following particle picking and image processing. Adding a proper chemical
20 reagent to reduce the interaction between the molecule and the air-water interface would
21 be an alternative way. In such case, the reaction constant k_1 in equation (2) is much

1 smaller than k_2 , and thus large portion of molecules are kept in the solution. Using
2 chemical cross-linker to increase the structural stability of bio-macromolecules would be
3 an additional way that the denaturing reaction constant k_3 is reduced.

4 **2.2 Conformational heterogeneity**

5 Cryo-EM SPA assumes that all the bio-macromolecules analyzed in the electron
6 micrographs have an identical structure and conformation. However, this assumption is not
7 rigorously true in most cases because of the unavoidable thermodynamics of bio-
8 macromolecules and would become much worse when there are heterogeneities existing
9 in the sample.

10 There are two kinds of heterogeneities of bio-macromolecules, the composition
11 heterogeneity and the conformational heterogeneity. The composition heterogeneity refers
12 to the specimen composed of a mixture of molecules with different ligand-bound states
13 [69], a mixture of macromolecular complexes with different subunits stoichiometry, a
14 mixture of macromolecular assembly with different symmetries, or even in a worst case a
15 mixture of the target molecule and contaminations. The conformational heterogeneity
16 refers to the specimen containing the target bio-macromolecules but in different functional
17 states, and can be further divided into two cases, the heterogeneity with discrete
18 conformations [93] and the one with continuous conformations [21].

19 The existence of heterogeneity will add difficulty in image processing of SPA and
20 prevent achieving high resolution structure. The composition heterogeneity can be possibly

1 and efficiently solved by improving biochemical preparation procedure, e.g. more specific
2 affinity chromatography. In addition, recent image processing algorithms have been well
3 developed by applying sophisticated statistics tools, e.g. principal component analysis [81,
4 82], maximum log likelihood [76] and Bayesian method [67]. Utilizing these advanced
5 image processing tools, we are able to perform efficient image classification to separate
6 bio-macromolecular particles with different compositions and solve the composition
7 heterogeneity [84].

8 The conformational heterogeneity reflects the functional and thermodynamics nature of
9 bio-macromolecules, which could not be easily improved by conventional biochemical
10 approaches. For the case of discrete conformations, the current image classification
11 algorithms can work very well if SNR of the particles are large enough to discriminate the
12 different conformations. However, for the case of continuous conformations, it would be
13 difficult to improve the reconstruction resolution by carrying out 3D classification
14 approaches unless incredible large number of particles are collected. There have been a
15 few image processing approaches developed to try to solve the heterogeneity of
16 continuous conformations, including local optimization refinement [73], masked refinement
17 [4], normal mode method [40] and manifold-embedding method [25]. When using local
18 optimization or masked refinement approach, we assumed that the bio-macromolecular
19 particle can be divided into a number of rigid parts and the relative orientations and
20 positions of different rigid parts contribute to the flexibility of the molecular complex. This
21 assumption worked in many cases to improve the resolution of bio-macromolecular flexible

1 modules [87]. However, it is not always true and the internal conformational changes of
2 different modules should be also considered in many cases.

3 The recent proposed normal mode and manifold-embedding methods would be good
4 solutions to study the intrinsic conformational dynamics of bio-macromolecules directly
5 from the raw cryo-EM images of bio-macromolecular particles. The normal mode method
6 first performs atomization of cryo-EM map and then calculates various normal modes of
7 clustered pseudo atoms. The specific modes are selected to simulate cryo-EM maps with
8 continuous conformations, which are then compared with the raw cryo-EM images[40, 66,
9 77].

10 The manifold-embedding method maps each projection of bio-macromolecule into a
11 point of hyperspace ($N \times N$ dimension, N is the size of projection image). All the points of
12 bio-macromolecules with different orientations and conformations will build a manifold in
13 this hyperspace. The dimension of this manifold is determined by the degree of freedom of
14 bio-macromolecular motion including rotation (3 freedoms), shift (2 freedoms) and
15 conformational changes (various freedoms). Manifold-embedding is a kind of mathematical
16 approach to estimate the degree of freedom of the manifold and decompose these
17 freedoms into different principal coordinates. After decomposition, a specific coordinate
18 can be selected and sorted to reconstruct the conformational changes of bio-
19 macromolecules [15, 25, 71, 72].

20 The recent published review [41] has discussed various image processing algorithms
21 to solve the conformational heterogeneity, especially the continuous conformation problem.

1 Besides the image processing approaches, here, I would like to propose another
2 biochemical approach to reduce the conformational heterogeneity of bio-macromolecules.

3 According to the Boltzmann's distribution law, the number of bio-macromolecules at a
4 specific state, N_c , is proportional to $e^{-\frac{E_c}{k_B T}}$, where E_c is the Gibbs energy of the bio-
5 macromolecule in this state c , and k_B is the Boltzmann constant (8.62E-5 eV/K), T is the
6 temperature of the bio-macromolecule solution. Suppose the lowest Gibbs energy of the
7 state is E_L (normally this state is called steady state and it is not degenerative, i.e., only
8 one conformation corresponds to this state), and the highest Gibbs energy of the state is
9 E_H (normally this state is degenerative, i.e., only multiple conformations correspond to this
10 state), the ratio of numbers of molecules between these two states can be determined as,

$$11 \quad r(T) = \frac{N_L}{N_H} = e^{\frac{E_H - E_L}{k_B T}} = e^{\frac{\Delta E}{k_B T}} \quad (3)$$

12 The Gibbs energy difference ΔE between two states of bio-macromolecules is 40~90 meV
13 [15, 21]. Then the ratio of the numbers can be estimated as, $r(298K) = 4.7 \sim 33.2$ (room
14 temperature), $r(277.6K) = 5.3 \sim 43.0$ (4 degree), $r(253.6K) = 6.2 \sim 61.4$ (-20 degree),
15 $r(193.6K) = 11.0 \sim 219.9$ (-80 degree). Therefore, if we could use chemical cross-linker
16 to fix the steady state at the low temperature (e.g. -20 or -80 degree) before vitrification,
17 there will be more populations of homogenous bio-macromolecular particles of the steady
18 state in the cryo-EM images, which provides an alternative approach to solve the
19 conformational heterogeneity. To utilize this approach, we need to add glycerol or other
20 cryo-protectants into the bio-macromolecular solution in order to keep the solution in liquid

1 state at low temperature, so that the thermodynamics equilibrium can be reached. Then
2 the chemical cross-linker is added to the cooled solution to allow the cross-linking reaction
3 occur. A good cross-linker needs to be screened and optimized to allow an efficient and
4 fast reaction at low temperature.

5 **2.3 Thick specimen and focus gradient**

6 The current image processing procedure of cryo-EM SPA assumes that the specimen
7 is thin enough so that the dynamic scattering, the Edward sphere and focus gradient effects
8 can be neglected. For 300 kV accelerate voltage and 100 nm thickness of vitrified bio
9 specimen, the dynamic scattering effect can be still neglected because it is smaller than
10 the mean free path (~ 350 nm) of 300 keV electron for the vitrified bio specimen [88].
11 However, the Edward sphere effect has limited the resolution to 3.8 angstrom according to
12 the formula of $\sqrt{t * \lambda / (2 * 0.7)}$, where t is the specimen thickness and λ ($= 0.02 \text{ \AA}$) is the
13 wavelength of 300 keV electron [16]. The 100 nm focus gradient will induce a phase error
14 of $\frac{\pi}{2}$ at the resolution of 6.3 angstrom according to the formula of $\Delta\chi = \pi\lambda\Delta Zs^2$, where $\Delta\chi$
15 is the phase error and ΔZ is the focus gradient [92]. Thus, when the size of bio-
16 macromolecule or the vitrified ice is thick, the Edward sphere, especially the focus gradient
17 will take effects and should be corrected to improve the resolution. In cryo-EM, the Edward
18 sphere and focus gradient effects are combined and corrections of these two effects are
19 actually equivalent [16].

20 Theory of Edward sphere correction has been well developed [16] and various
21 algorithms have been implemented into difference programs and tested with simulated

1 data [47, 86]. The effect of focus gradient was also carefully discussed recently using
 2 simulated data [20]. Here, I will discuss the focus gradient effect in a different way and
 3 provide a new approximation to solve and correct this effect.

4 As shown in **Figure 3**, suppose the thickness of the specimen is D , the underfocus of
 5 the proximal side is f_0 , and that of the distal side is $f_0 + D$, the averaged underfocus of
 6 the specimen is $f_a = f_0 + D/2$. For the thin specimen, the final image can be simply
 7 formulated as,

$$8 \quad I(x, y) = p(x, y) \otimes PSF(f_a, x, y) \quad (4)$$

9 where, $p(x, y)$ is the projection of the structural density $f(x, y, z)$ of the specimen,

$$10 \quad p(x, y) = \int_{f_0}^{f_0+D} f(x, y, z) dz \quad (5)$$

11 and $PSF(f_a, x, y)$ is the point spread function of the objective lens, and is the Fourier
 12 transformation of contrast transfer function,

$$13 \quad CTF(f_a, s_x, s_y) = \text{Sin}\chi(f_a, s) = \text{Sin}\left(\frac{\pi}{2} \lambda C_s^3 s^4 - \pi \lambda f_a s^2\right) \quad (6)$$

14 For simplicity, here we do not consider astigmatism and amplitude contrast and therefore
 15 $s^2 = s_x^2 + s_y^2$.

16 However, when the thickness D is large enough, equation (4) has to be corrected by
 17 dividing the specimen into a series of thin specimen ($n=0, 1, 2, \dots, N-1$), thus the the final
 18 image of a thick specimen can be formulated as,

$$1 \quad I(x, y) = \sum_{n=0}^{N-1} \Delta z * f(x, y, f_0 + n\Delta z) \otimes PSF(f_0 + n\Delta z, x, y) \quad (7)$$

2 When $N \rightarrow +\infty$, we have,

$$3 \quad I(x, y) = \int_{f_0}^{f_0+D} f(x, y, f_0 + z) \otimes PSF(f_0 + z, x, y) dz$$

$$4 \quad = \int_{-\frac{D}{2}}^{\frac{D}{2}} f(x, y, f_a + z) \otimes PSF(f_a + z, x, y) dz \quad (8)$$

5 Considering $D (\sim 100 \text{ nm}) \ll f_a (1000 \sim 2500 \text{ nm})$, the point spread function can be
6 expanded at $z = 0$ and approximated as,

$$7 \quad PSF(f_a + z, x, y) = PSF(f_a, x, y) + z * \frac{\partial PSF}{\partial z} \Big|_{z=0} \quad (9)$$

8 Combining (8) and (9), we have,

$$9 \quad I(x, y) = I^0(x, y) + I^1(x, y) \quad (10)$$

$$10 \quad I^0(x, y) = \int_{-\frac{D}{2}}^{\frac{D}{2}} f(x, y, f_a + z) dz \otimes PSF(f_a, x, y) \quad (11)$$

$$11 \quad I^1(x, y) = \int_{-\frac{D}{2}}^{\frac{D}{2}} f(x, y, f_a + z) z dz \otimes \frac{\partial PSF}{\partial z} \Big|_{z=0} \quad (12)$$

12 Next, we consider Fourier transformation of the structural density $f(x, y, z)$ of the
13 specimen,

$$14 \quad F(s_x, s_y, s_z) = \iint \int_{-\frac{D}{2}}^{\frac{D}{2}} f(x, y, f_a + z) * e^{-i\pi(xs_x + ys_y + zs_z)} dz dx dy \quad (13)$$

15 Thus, we have the projection theorem,

$$\begin{aligned}
1 \quad F(s_x, s_y, 0) &= \iint \int_{z=-\frac{D}{2}}^{\frac{D}{2}} f(x, y, f_a + z) dz * e^{-i\pi(x s_x + y s_y)} dx dy \\
2 \quad &= \iint p(x, y) * e^{-i\pi(x s_x + y s_y)} dx dy \quad (14)
\end{aligned}$$

3 and the following relationship,

$$\begin{aligned}
4 \quad \frac{\partial F}{\partial s_z} \Big|_{s_z=0} &= \int f(x, y, f_a + z) * e^{-i\pi(x s_x + y s_y + z s_z)} * (-i\pi z) dx dy dz \Big|_{s_z=0} \\
5 \quad &= \iint \frac{\pi}{i} \int_{z=-\frac{D}{2}}^{\frac{D}{2}} f(x, y, f_a + z) z dz * e^{-i\pi(x s_x + y s_y)} dx dy \quad (15)
\end{aligned}$$

6 As a result, combining (14) and (15) and utilizing the convolution theorem, the Fourier
7 transformation of equation (10) becomes,

$$8 \quad \hat{I}(s_x, s_y) = F(s_x, s_y, 0) * CTF(f_a, s) + \frac{i}{\pi} \frac{\partial F}{\partial s_z} \Big|_{s_z=0} * \frac{\partial CTF(f_a + z, s)}{\partial z} \Big|_{z=0} \quad (16)$$

9 Combining (6) and (16), we have,

$$10 \quad \hat{I}(s_x, s_y) = F(s_x, s_y, 0) * \text{Sin } \chi(f_a, s) - i\lambda \left(\frac{\partial F}{\partial s_z} \right)_{s_z=0} * \text{Cos } \chi(f_a, s) * s^2 \quad (17)$$

11 From (17), it is clear to see, for the thick specimen, the Fourier transformation of cryo-EM
12 image contains an additional term $i\lambda \left(\frac{\partial F}{\partial s_z} \right)_{s_z=0} * \text{Cos } \chi(f_a, s) * s^2$. This term has a minor
13 contribution at the low resolution but will interfere significantly with the first term and induce
14 Thron ring fading out at the high resolution.

15 Equation (17) provides at least two ways to solve and correct the focus gradient effect.

16 For the first way, we can take two cryo-EM images of the same specimen with different

1 underfocus, yielding two equations. The underfocus parameters can be accurately
2 estimated by fitting Thron ring and using the low resolution data. Then the structural factor
3 $F(s_x, s_y, 0)$ can be solved directly. The concern of reduced SNR from additional radiation
4 damage of the second exposure has been discussed carefully and can be eliminated [16].

5 The second way does not need two experimental images but apply an iterative
6 algorithm to solve the structural factor. Initially, the second term of (17) is neglected and
7 normal cryo-EM SPA procedure is performed to get the first round of structure. Then $\frac{\partial F}{\partial s_z}$
8 can be computed and will be used to update the structural factor $F(s_x, s_y, 0)$ according to
9 (17). Therefore, the structure of cryo-EM map can be reconstructed again with an improved
10 resolution. This procedure can be iterated several rounds until the convergence reaches.

11 **2.4 Beam induced motion and radiation damage**

12 Cryo-EM of bio-macromolecules embedded in vitreous ice has suffered from beam
13 induced motion (BIM) for many years. When accelerated high-energy electrons interact
14 with the specimen, the electrons from the specimen will be scattered and become
15 secondary electrons coming out of the specimen, leaving positively charged annulus at the
16 illumination area [9]. This is called charging effect ('Berriman effect') from electron beam
17 illumination. Since the thin layer of vitreous ice is an insulator, the positive charges can not
18 be quickly compensated from the environment and thus induce the subsequent physical
19 effects. First, the irregular and metastable structure of the vitrified ice can easily response
20 to the internal electrostatic repulsion stress from the positive charges and thus result a

1 global mechanical deformation. Such global mechanical deformation is much significant at
2 the beginning of electron illumination [48] and was observed to have a dome-like shape [8].
3 The mechanical deformation of the ice layer during electron illumination will result a blurred
4 cryo-EM image and weaken the high resolution information significantly. Second, the
5 positive charged annulus will induce additional phase shift of electron beam just like a
6 microscopic electrostatic lens, which will induce an additional contrast loss and blurring of
7 the final image [9], which, however and fortunately, has the minimal effect on the high
8 resolution cryo-EM SPA technique according to the recent study [63].

9 Besides charging effect that causes BIM, electron beam illumination will induce another
10 more severe effect, which is called radiation damage (or radiolysis). When the secondary
11 electron is kicked out, the chemical covalent bond of molecule will be broken, generating
12 many free-radicals. The free-radicals can migrate quickly and react with the adjacent
13 molecules. As a result, the structure of bio-macromolecule can be damaged effectively
14 from the electron beam illumination and the high resolution structural information will be
15 damped significantly when the illumination dose increased [32, 34]. Thus, electron
16 radiation damage must be carefully considered and the electron dose should be carefully
17 controlled for high resolution cryo-EM SPA work.

18 The electron radiation damage of vitreous ice embedded bio-macromolecules will
19 further cause the 'bubbling' effect that is routinely observed in cryo-EM experiments. Since
20 both water molecules and bio-macromolecules contain abundant hydrogen atoms, electron
21 radiolysis will generate large amount of hydrogen free-radicals and these hydrogen free-

1 radicals will react subsequently to form hydrogen molecule [46]. At the interfaces between
2 bio-macromolecules and ice or the support carbon film and ice, hydrogen molecules are
3 frequently accumulated into a high concentration and form the hydrogen gas pocket, which
4 was observed as the 'bubbling' effect [12]. The generation of hydrogen gas pocket will
5 produce additional mechanical stress within the cryo-vitrified specimen and thus become
6 another factor of BIM. By using a very low electron radiation dose-rate, the accumulation
7 of hydrogen gas can be effectively decreased and thus the 'bubbling' effect can be
8 alleviated [12]. To be noted, the 'bubbling' effect used to be developed as a kind of
9 technique to study the internal nucleic structure of virus [13].

10 Recently, another kind of BIM effect, called beam-induced Brownian motion, was
11 proposed and studied [54]. This effect describes a pseudo-Brownian motion of vitreous ice
12 embedded bio-macromolecules, which is generated from the beam-induced movement of
13 water molecules. Fortunately, the experimental data and simulation study by Henderson
14 and coworkers suggested that this beam-induced Brownian motion has the minimal effect
15 on the current cryo-EM SPA work unless the size of bio-macromolecule is small and the
16 target resolution goes beyond 2 angstrom [54].

17 The existence of BIM and electron radiation damage has been aware of the key
18 bottleneck of high resolution cryo-EM SPA for many years until the emerging of the direct
19 electron detector (DED) [39]. The high detective quantum efficiency (DQE) of the DED
20 camera [53] allows to retain the high resolution weak signal under low dose electron
21 radiation that is important to reduce radiation damage of bio-macromolecules. Equally

1 importantly, the CMOS architecture of DEM camera enables a high frame rate to record a
2 single exposure into a movie, which can be utilized to correct BIM efficiently by applying
3 appropriate image processing algorithms [8, 48, 94]. In addition, by using dose
4 fractionation and damage compensation algorithms, the movie mode of DED camera can
5 further allow to use a high illumination dose to take cryo-EM images for a better contrast
6 [32].

7 Besides the direct electron detector that can correct BIM during image processing
8 procedure, additional efforts have been also performed to alleviate BIM effect and these
9 include spot scan imaging [10, 19], paraxial charge compensator [5], and development of
10 various supporting films such Cryo-Mesh grid, graphene film and pure gold grid [64, 65,
11 89]. The pure gold grid was proved to have sufficient mechanical stiffness and good
12 conductivity, which can therefore reduce BIM [65] and has been successfully applied in
13 many high resolution cryo-EM SPA applications [17].

14 Overall, the efforts of developing direct electron detector, motion correction algorithms
15 and new types of supporting films in recent years have significantly reduce the effects from
16 BIM and electron radiation damage. More and more bio-macromolecular structures are
17 solved to near atomic resolution (3 ~ 4 angstrom) by cryo-EM SPA approach. However, the
18 electron radiation damage effect is still existing and will be the most important bottleneck
19 of cryo-EM SPA in the future to achieve atomic resolution. Previous studies have showed
20 that the high resolution (~ 3 angstrom) information of vitreous embedded biological
21 specimen already falls off after a low dose ($3 e / \text{\AA}^2$) of electron radiation[34]. The severe

1 mechanical deformation of ice layer at the first dose fractionated frames could not be
 2 corrected by image processing algorithms [48]. As a result, while the first couple of frames
 3 with less radiation damage contains atomic resolution information, this information can not
 4 be restored due to a large BIM and thus these frames have to be discarded in the
 5 subsequent image processing.

6 In the future, there will be two potential ways to further alleviate the electron radiation
 7 damage effect. The first possible way is to utilize quantum entanglement effect of electrons
 8 to reduce the shot noise of electron beam from the normal scale $\sim 1/N^{1/2}$ to the
 9 Heisenberg limit $\sim 1/N$ [27, 56]. As a result, we could utilize a even low electron dose
 10 ($1 e / \text{\AA}^2$) to capture a good image with enough SNR and less radiation damage [56]. The
 11 another possible way is to consider the time scale of electron radiation damage. If we could
 12 take cryo-EM image before the specimen damage occurs, we thus could have an
 13 opportunity of obtaining the damage-free and high resolution structure of bio-
 14 macromolecule. This idea has been proved in the field of serial femtosecond X-ray
 15 crystallography with the term of 'diffraction before damage' [51]. In cryo-EM of bio-
 16 macromolecules, it is important to estimate the time scale of specimen damage from
 17 electron radiation and then verify the possibility of the term of 'imaging before damage'.

18 For 300kV transmission electron microscope, the accelerated electron gains a high

19 speed $v = c \sqrt{1 - \frac{1}{(1+E/E_0)^2}} = 0.78c = 2.3 \times 10^8 m/s$, where the relativistic effect has to be

20 considered, the static energy of electron is $E_0 = m_0c^2 = 511keV$, the kinetic energy is $E =$

1 300keV and the light speed in vacuum is $c = 3 \times 10^8 \text{ m/s}$. Then, the time for an electron
2 traveling across a specimen with the thickness of $d = 100 \text{ nm}$ is $\Delta t = \frac{d}{v} = 0.33 \text{ fs}$. Thus,
3 we could estimate the time scale of the interaction between the specimen and the high
4 energy electron is $\sim 1 \text{ fs}$. Then there will be many damage events occurred in the
5 biological specimen, which can be divided into two processes, the primary damage process
6 and the secondary damage process [30, 38]. The primary damage process includes
7 chemical bond breaking, ionization, and production of secondary electrons and free
8 radicals. Previous studies suggested that the time scale of the primary damage process is
9 $1\sim 10 \text{ ps}$ and such damage does not influence the electron microscopic image appreciably
10 [70], because the positions of atoms do not change noticeably at this time scale. The only
11 detectable damage in the electron microscopic image occurs in the secondary process,
12 which initiates from the transition of free radicals and includes subsequent cascade
13 reactions induced by free radicals and productions of new chemical bonds. During the
14 second process, the positions of atoms in the specimen have changed significantly,
15 resulting appreciable damage effect in the final electron microscopic image. The time scale
16 of the second process depends on the rate of free radical transition, which can be
17 estimated as below.

18 As discussed above, the abundant free radicals generated from vitreous ice embedded
19 bio-macromolecules are hydrogen free radicals H^* . The transition of H^* follows the Fick's
20 laws of diffusion,

$$21 \quad J = vC = -D \cdot \frac{dC}{dx} \quad (18)$$

1 where, v is the transition rate of H^* , C is the local concentration of H^* , the diffusion
 2 coefficient can be calculated according to Stokes-Einstein relationship,

$$3 \quad D = \frac{k_B T}{6\pi\eta r} \quad (19)$$

4 where, k_B is the Boltzmann constant (1.38×10^{-23} J/K), T is the temperature of vitrified
 5 specimen, η is the viscosity of the vitreous ice, and r ($\sim 10^{-10}$ m) is the radius of H^* .
 6 Combining (18) and (19), we can calculate the transition rate of H^* as,

$$7 \quad v = \frac{1}{C} \cdot \frac{k_B T}{6\pi\eta r} \cdot \frac{dC}{dx} \quad (20)$$

8 Suppose, initially, the free radicals H^* are concentrated in a small cubic region with the
 9 size of 1 nm^3 , thus we could have the following estimation,

$$10 \quad \frac{1}{C} \cdot \frac{dC}{dx} = \frac{1}{C} \cdot \frac{\Delta C}{\Delta x} \sim \frac{1}{\Delta x} \sim 10^9 \text{ m}^{-1} \quad (21)$$

11 Thus, at the temperature ($T = 90 \text{ K}$) of cryo-EM experiments, the transition rate of H^* can
 12 be estimated as,

$$13 \quad v \sim \frac{1.38 \times 10^{-23} \times 90}{6 \times 3.14 \times 10^{-3} \times 10^{-10}} \times 10^9 = 0.7 \text{ m/s} \quad (22)$$

14 Then the time for H^* traveling 0.3 nm , the averaged distance to reach adjacent groups
 15 and then perform radical reaction, can be estimated as,

$$16 \quad \Delta t \sim \frac{0.3 \text{ nm}}{0.7 \text{ m/s}} = 0.4 \text{ ns} \quad (23)$$

17 To be noted that, the estimation in (22) utilizes the water viscosity at room temperature,

1 $\eta_{H_2O} = 10^{-3} Pa \cdot s$, where the viscosity of the vitreous ice η_{ice} at 90 K should be much
2 larger (e.g. more than ten times) than the water viscosity at room temperature. Therefore,
3 the time scale for the second damage process is in the nanoseconds $\sim 10 ns$.

4 The above estimation suggests that if we could take a cryo-EM exposure within 10 ns,
5 the appreciable electron radiation damage during the second process can be almost
6 avoided in the final recorded micrograph. The recent developed ultrafast transmission
7 electron microscopy (UEM) [11, 26, 75, 91] has actually provided an opportunity to test this
8 kind of idea. There are two operation modes of UEM, the stroboscopic mode with
9 picosecond temporal resolution and the single-pulse mode with nanosecond temporal
10 resolution [75]. The stroboscopic mode is useful for ultrafast electron diffraction
11 experiments and suitable to study the reversible process of the material. However, the
12 electron radiation damage of bio-macromolecules is irreversible. Thus, to achieve the
13 concept of 'imaging before damage', it is necessary to develop the cryo-ultrafast
14 transmission electron microscopy (cryo-UEM) that is operated in the single-pulse mode.
15 Although there have been some reports of using UEM to observe the biological specimens
16 [22, 23, 50], all these studies were performed in the stroboscopic mode and utilized the
17 dehydrated specimen, which should not be relevant to biological functions. There is still a
18 big space to develop and improve the single-pulse UEM technology. We are looking
19 forward to the future maturation of cryo-UEM that will bring the bio-macromolecular
20 electron microscopy into a new era.

21

1 **3. Conclusions**

2 Cryo-EM SPA has become the most important technique of bio-macromolecular
3 electron microscopy. The era of studying the structures of bio-macromolecules by using
4 Cryo-EM SPA is just beginning. In the near future, we will see more and more sophisticated
5 bio-macromolecular complexes whose structures are solved into near atomic resolution,
6 making significant implications to their biological functions. However, just as Henderson
7 [36] and Glaeser [27] pointed, cryo-electron microscopy has not yet realized its full potential.
8 In the future, with a better cryo-vitrification technique to avoid air-water interface problem,
9 with a better camera and new type of microscope to further alleviate electron radiation
10 damage effect and with some novel image processing algorithms and experimental
11 techniques to solve the focus gradient problem as well as the conformational heterogeneity
12 issue, Cryo-EM SPA will expand its full ability to solve the atomic resolution of bio-
13 macromolecules.

14 **ACKNOWLEDGEMENTS**

15 I would like to apologize that there are also many other pioneer works of developing
16 bio-macromolecular electron microscopy, which are not mentioned in this review due to
17 limited space. I would like to thank Dr. Xiaojun Huang for her critical comments of the
18 manuscript, Shuangbo Zhang for his assistance of literatures searching, and Ping Shan
19 and Ruigang Su for their assistances in the lab management. This work is supported by
20 grants from Chinese Academy of Sciences (ZDKYYQ20170002 and XDB08030202) and
21 Ministry of Science and Technology of China (2017YFA0504700 and 2014CB910700).

References

- 1
- 2 [1] Adrian M, Dubochet J, Lepault J and McDowell A W 1984 Cryo-electron microscopy
3 of viruses *Nature* **308** 32-6
- 4 [2] Arnold S A, Albiez S, Bieri A, Syntychaki A, Adaixo R, McLeod R A, Goldie K N, Stahlberg
5 H and Braun T 2017 Blotting-free and lossless cryo-electron microscopy grid
6 preparation from nanoliter-sized protein samples and single-cell extracts *Journal of*
7 *structural biology* **197** 220-6
- 8 [3] Bai X C, Fernandez I S, McMullan G and Scheres S H 2013 Ribosome structures to near-
9 atomic resolution from thirty thousand cryo-EM particles *eLife* **2** e00461
- 10 [4] Bai X C, Rajendra E, Yang G, Shi Y and Scheres S H 2015 Sampling the conformational
11 space of the catalytic subunit of human gamma-secretase *eLife* **4**
- 12 [5] Berriman J A and Rosenthal P B 2012 Paraxial charge compensator for electron
13 cryomicroscopy *Ultramicroscopy* **116** 106-14
- 14 [6] Biyani N, Righetto R D, McLeod R, Caujolle-Bert D, Castano-Diez D, Goldie K N and
15 Stahlberg H 2017 Focus: The interface between data collection and data processing in
16 cryo-EM *Journal of structural biology* **198** 124-33
- 17 [7] Briggs J A 2013 Structural biology in situ--the potential of subtomogram averaging
18 *Curr Opin Struct Biol* **23** 261-7
- 19 [8] Brilot A F, Chen J Z, Cheng A, Pan J, Harrison S C, Potter C S, Carragher B, Henderson
20 R and Grigorieff N 2012 Beam-induced motion of vitrified specimen on holey carbon
21 film *Journal of structural biology* **177** 630-7
- 22 [9] Brink J, Sherman M B, Berriman J and Chiu W 1998 Evaluation of charging on
23 macromolecules in electron cryomicroscopy *Ultramicroscopy* **72** 41-52
- 24 [10] Bullough P and Henderson R 1987 Use of spot-scan procedure for recording low-dose
25 micrographs of beam-sensitive specimens *Ultramicroscopy* **21** 223-30
- 26 [11] Cao G, Sun S, Li Z, Tian H, Yang H and Li J 2015 Clocking the anisotropic lattice
27 dynamics of multi-walled carbon nanotubes by four-dimensional ultrafast
28 transmission electron microscopy *Scientific reports* **5** 8404
- 29 [12] Chen J Z, Sachse C, Xu C, Mielke T, Spahn C M and Grigorieff N 2008 A dose-rate
30 effect in single-particle electron microscopy *Journal of structural biology* **161** 92-100
- 31 [13] Cheng N, Wu W, Watts N R and Steven A C 2014 Exploiting radiation damage to map
32 proteins in nucleoprotein complexes: the internal structure of bacteriophage T7

- 1 *Journal of structural biology* **185** 250-6
- 2 [14] Cheng Y 2015 Single-Particle Cryo-EM at Crystallographic Resolution *Cell* **161** 450-7
- 3 [15] Dashti A, Schwander P, Langlois R, Fung R, Li W, Hosseinizadeh A, Liao H Y, Pallesen J,
4 Sharma G, Stupina V A, Simon A E, Dinman J D, Frank J and Ourmazd A 2014
5 Trajectories of the ribosome as a Brownian nanomachine *Proc Natl Acad Sci U S A* **111**
6 17492-7
- 7 [16] DeRosier D J 2000 Correction of high-resolution data for curvature of the Ewald sphere
8 *Ultramicroscopy* **81** 83-98
- 9 [17] des Georges A, Clarke O B, Zalk R, Yuan Q, Condon K J, Grassucci R A, Hendrickson W
10 A, Marks A R and Frank J 2016 Structural Basis for Gating and Activation of RyR1 *Cell*
11 **167** 145-57 e17
- 12 [18] Downing K H 1988 Observations of restricted beam-induced specimen motion with
13 small-spot illumination *Ultramicroscopy* **24** 387-97
- 14 [19] Downing K H and Glaeser R M 1986 Improvement in high resolution image quality of
15 radiation-sensitive specimens achieved with reduced spot size of the electron beam
16 *Ultramicroscopy* **20** 269-78
- 17 [20] Downing K H and Glaeser R M 2017 Estimating the effect of finite depth of field in
18 single-particle cryo-EM *Ultramicroscopy* **184** 94-9
- 19 [21] Fischer N, Konevega A L, Wintermeyer W, Rodnina M V and Stark H 2010 Ribosome
20 dynamics and tRNA movement by time-resolved electron cryomicroscopy *Nature* **466**
21 329-33
- 22 [22] Fitzpatrick A W, Lorenz U J, Vanacore G M and Zewail A H 2013 4D cryo-electron
23 microscopy of proteins *Journal of the American Chemical Society* **135** 19123-6
- 24 [23] Fitzpatrick A W, Park S T and Zewail A H 2013 Exceptional rigidity and biomechanics
25 of amyloid revealed by 4D electron microscopy *Proc Natl Acad Sci U S A* **110** 10976-
26 81
- 27 [24] Frank J 1990 Classification of macromolecular assemblies studied as 'single particles'
28 *Quarterly reviews of biophysics* **23** 281-329
- 29 [25] Frank J and Ourmazd A 2016 Continuous changes in structure mapped by manifold
30 embedding of single-particle data in cryo-EM *Methods*
- 31 [26] Fu X, Chen B, Tang J, Hassan M T and Zewail A H 2017 Imaging rotational dynamics of
32 nanoparticles in liquid by 4D electron microscopy *Science (New York, N.Y)* **355** 494-8
- 33 [27] Glaeser R M 2016 How good can cryo-EM become? *Nature methods* **13** 28-32

- 1 [28] Glaeser R M and Han B G 2017 Opinion: hazards faced by macromolecules when
2 confined to thin aqueous films *Biophys Rep* **3** 1-7
- 3 [29] Glaeser R M, Han B G, Csencsits R, Killilea A, Pulk A and Cate J H 2016 Factors that
4 Influence the Formation and Stability of Thin, Cryo-EM Specimens *Biophys J* **110** 749-
5 55
- 6 [30] Glaeser R M and Taylor K A 1978 Radiation damage relative to transmission electron
7 microscopy of biological specimens at low temperature: a review *Journal of*
8 *microscopy* **112** 127-38
- 9 [31] Gonen T, Cheng Y, Sliz P, Hiroaki Y, Fujiyoshi Y, Harrison S C and Walz T 2005 Lipid-
10 protein interactions in double-layered two-dimensional AQP0 crystals *Nature* **438**
11 633-8
- 12 [32] Grant T and Grigorieff N 2015 Measuring the optimal exposure for single particle cryo-
13 EM using a 2.6 Å reconstruction of rotavirus VP6 *eLife* **4** e06980
- 14 [33] Grigorieff N 2016 FREALIGN: An Exploratory Tool for Single-Particle Cryo-EM *Methods*
15 *Enzymol* **579** 191-226
- 16 [34] Hayward S B and Glaeser R M 1979 Radiation damage of purple membrane at low
17 temperature *Ultramicroscopy* **04** 201-10
- 18 [35] Henderson R 1995 The potential and limitations of neutrons, electrons and X-rays for
19 atomic resolution microscopy of unstained biological molecules *Quarterly reviews of*
20 *biophysics* **28** 171-93
- 21 [36] Henderson R 2015 Overview and future of single particle electron cryomicroscopy *Arch*
22 *Biochem Biophys*
- 23 [37] Henderson R and Unwin P N 1975 Three-dimensional model of purple membrane
24 obtained by electron microscopy *Nature* **257** 28-32
- 25 [38] Hendrickson W A 1976 Radiation damage in protein crystallography *Journal of*
26 *molecular biology* **106** 889-93
- 27 [39] Jin L, Milazzo A C, Kleinfelder S, Li S, Leblanc P, Duttweiler F, Bouwer J C, Peltier S T,
28 Ellisman M H and Xuong N H 2008 Applications of direct detection device in
29 transmission electron microscopy *Journal of structural biology* **161** 352-8
- 30 [40] Jin Q, Sorzano C O, de la Rosa-Trevin J M, Bilbao-Castro J R, Nunez-Ramirez R, Llorca
31 O, Tama F and Jonic S 2014 Iterative elastic 3D-to-2D alignment method using normal
32 modes for studying structural dynamics of large macromolecular complexes *Structure*
33 **22** 496-506

- 1 [41] Jonic S 2017 Computational methods for analyzing conformational variability of
2 macromolecular complexes from cryo-electron microscopy images *Curr Opin Struct*
3 *Biol* **43** 114-21
- 4 [42] Kelly D F, Dukovski D and Walz T 2010 Strategy for the use of affinity grids to prepare
5 non-His-tagged macromolecular complexes for single-particle electron microscopy
6 *Journal of molecular biology* **400** 675-81
- 7 [43] Khoshouei M, Pfeffer S, Baumeister W, Forster F and Danev R 2016 Subtomogram
8 analysis using the Volta phase plate *Journal of structural biology*
- 9 [44] Khoshouei M, Radjainia M, Phillips A J, Gerrard J A, Mitra A K, Plitzko J M, Baumeister
10 W and Danev R 2016 Volta phase plate cryo-EM of the small protein complex Prx3
11 *Nat Commun* **7** 10534
- 12 [45] Kuhlbrandt W 2014 Biochemistry. The resolution revolution *Science (New York, N.Y)*
13 **343** 1443-4
- 14 [46] Leapman R D and Sun S 1995 Cryo-electron energy loss spectroscopy: observations
15 on vitrified hydrated specimens and radiation damage *Ultramicroscopy* **59** 71-9
- 16 [47] Leong P A, Yu X, Zhou Z H and Jensen G J 2010 *Methods in Enzymology*, ed J J Grant:
17 Academic Press) pp 369-80
- 18 [48] Li X, Mooney P, Zheng S, Booth C R, Braunfeld M B, Gubbens S, Agard D A and Cheng
19 Y 2013 Electron counting and beam-induced motion correction enable near-atomic-
20 resolution single-particle cryo-EM *Nature methods*
- 21 [49] Liao M, Cao E, Julius D and Cheng Y 2013 Structure of the TRPV1 ion channel
22 determined by electron cryo-microscopy *Nature* **504** 107-12
- 23 [50] Lorenz U J and Zewail A H 2013 Biomechanics of DNA structures visualized by 4D
24 electron microscopy *Proc Natl Acad Sci U S A* **110** 2822-7
- 25 [51] Martin-Garcia J M, Conrad C E, Coe J, Roy-Chowdhury S and Fromme P 2016 Serial
26 femtosecond crystallography: A revolution in structural biology *Arch Biochem Biophys*
27 **602** 32-47
- 28 [52] Mastronarde D 2003 SerialEM A Program for Automated Tilt Series Acquisition on
29 Tecnai Microscopes Using Prediction of Specimen Position *Microscopy and*
30 *Microanalysis* **9** 1182-3
- 31 [53] McMullan G, Faruqi A R, Clare D and Henderson R 2014 Comparison of optimal
32 performance at 300keV of three direct electron detectors for use in low dose electron
33 microscopy *Ultramicroscopy* **147** 156-63

- 1 [54] McMullan G, Vinothkumar K R and Henderson R 2015 Thon rings from amorphous ice
2 and implications of beam-induced Brownian motion in single particle electron cryo-
3 microscopy *Ultramicroscopy* **158** 26-32
- 4 [55] Merk A, Bartesaghi A, Banerjee S, Falconieri V, Rao P, Davis M I, Pragani R, Boxer M B,
5 Earl L A, Milne J L and Subramaniam S 2016 Breaking Cryo-EM Resolution Barriers to
6 Facilitate Drug Discovery *Cell* **165** 1698-707
- 7 [56] Okamoto H 2012 Possible use of a Cooper-pair box for low-dose electron microscopy
8 *Physical Review A* **85** 043810
- 9 [57] Orlova E V and Saibil H R 2011 Structural analysis of macromolecular assemblies by
10 electron microscopy *Chem Rev* **111** 7710-48
- 11 [58] Patwardhan A 2017 Trends in the Electron Microscopy Data Bank (EMDB) *Acta*
12 *Crystallogr D Struct Biol* **73** 503-8
- 13 [59] Punjani A, Rubinstein J L, Fleet D J and Brubaker M A 2017 cryoSPARC: algorithms for
14 rapid unsupervised cryo-EM structure determination *Nature methods*
- 15 [60] Quinn P J and Dawson R M 1970 An analysis of the interaction of protein with lipid
16 monolayers at the air-water interface *Biochem J* **116** 671-80
- 17 [61] Razinkov I, Dandey V, Wei H, Zhang Z, Melnekoff D, Rice W J, Wigge C, Potter C S and
18 Carragher B 2016 A new method for vitrifying samples for cryoEM *Journal of structural*
19 *biology* **195** 190-8
- 20 [62] Rosenthal P B and Henderson R 2003 Optimal determination of particle orientation,
21 absolute hand, and contrast loss in single-particle electron cryomicroscopy *Journal of*
22 *molecular biology* **333** 721-45
- 23 [63] Russo C J and Henderson R 2018 Microscopic charge fluctuations cause minimal
24 contrast loss in cryoEM *Ultramicroscopy* **187** 56-63
- 25 [64] Russo C J and Passmore L A 2014 Controlling protein adsorption on graphene for
26 cryo-EM using low-energy hydrogen plasmas *Nature methods*
- 27 [65] Russo C J and Passmore L A 2016 Ultrastable gold substrates: Properties of a support
28 for high-resolution electron cryomicroscopy of biological specimens *Journal of*
29 *structural biology* **193** 33-44
- 30 [66] Sanchez Sorzano C O, Alvarez-Cabrera A L, Kazemi M, Carazo J M and Jonic S 2016
31 StructMap: Elastic Distance Analysis of Electron Microscopy Maps for Studying
32 Conformational Changes *Biophys J* **110** 1753-65
- 33 [67] Scheres S H 2012 A Bayesian view on cryo-EM structure determination *Journal of*

- 1 *molecular biology* **415** 406-18
- 2 [68] Scheres S H 2012 RELION: implementation of a Bayesian approach to cryo-EM
3 structure determination *Journal of structural biology* **180** 519-30
- 4 [69] Scheres S H, Gao H, Valle M, Herman G T, Eggermont P P, Frank J and Carazo J M 2007
5 Disentangling conformational states of macromolecules in 3D-EM through likelihood
6 optimization *Nature methods* **4** 27-9
- 7 [70] Schnabl H 1980 Does removal of hydrogen change the electron energy-loss spectra
8 of DNA bases? *Ultramicroscopy* **5** 147-51
- 9 [71] Schwander P, Fung R, G. N. Phillips J and Ourmazd A 2010 Mapping the conformations
10 of biological assemblies *New Journal of Physics* **12** 035007
- 11 [72] Schwander P, Fung R and Ourmazd A 2014 Conformations of macromolecules and
12 their complexes from heterogeneous datasets *Philos Trans R Soc Lond B Biol Sci* **369**
13 20130567
- 14 [73] Shan H, Wang Z, Zhang F, Xiong Y, Yin C C and Sun F 2016 A local-optimization
15 refinement algorithm in single particle analysis for macromolecular complex with
16 multiple rigid modules *Protein & cell* **7** 46-62
- 17 [74] Shi D, Nannenga B L, Iadanza M G and Gonen T 2013 Three-dimensional electron
18 crystallography of protein microcrystals *eLife* **2** e01345
- 19 [75] Shorokhov D and Zewail A H 2016 Perspective: 4D ultrafast electron microscopy-
20 Evolutions and revolutions *J Chem Phys* **144** 080901
- 21 [76] Sigworth F J, Doerschuk P C, Carazo J M and Scheres S H 2010 An introduction to
22 maximum-likelihood methods in cryo-EM *Methods Enzymol* **482** 263-94
- 23 [77] Sorzano C O, de la Rosa-Trevin J M, Tama F and Jonic S 2014 Hybrid Electron
24 Microscopy Normal Mode Analysis graphical interface and protocol *Journal of*
25 *structural biology* **188** 134-41
- 26 [78] Suloway C, Pulokas J, Fellmann D, Cheng A, Guerra F, Quispe J, Stagg S, Potter C S and
27 Carragher B 2005 Automated molecular microscopy: the new Legion system *Journal*
28 *of structural biology* **151** 41-60
- 29 [79] Taylor K A and Glaeser R M 1974 Electron diffraction of frozen, hydrated protein
30 crystals *Science (New York, N.Y)* **186** 1036-7
- 31 [80] Thompson R F, Walker M, Siebert C A, Muench S P and Ranson N A 2016 An
32 introduction to sample preparation and imaging by cryo-electron microscopy for
33 structural biology *Methods* **100** 3-15

- 1 [81] van Heel M 1984 Multivariate statistical classification of noisy images (randomly
2 oriented biological macromolecules) *Ultramicroscopy* **13** 165-83
- 3 [82] Van Heel M and Frank J 1981 Use of multivariate statistics in analysing the images of
4 biological macromolecules *Ultramicroscopy* **6** 187-94
- 5 [83] Vinothkumar K R, Zhu J and Hirst J 2014 Architecture of mammalian respiratory
6 complex I *Nature* **advance online publication**
- 7 [84] Voorhees R M, Fernandez I S, Scheres S H and Hegde R S 2014 Structure of the
8 mammalian ribosome-Sec61 complex to 3.4 Å resolution *Cell* **157** 1632-43
- 9 [85] Wei X, Su X, Cao P, Liu X, Chang W, Li M, Zhang X and Liu Z 2016 Structure of spinach
10 photosystem II-LHCII supercomplex at 3.2 Å resolution *Nature* **534** 69-74
- 11 [86] Wolf M, DeRosier D J and Grigorieff N 2006 Ewald sphere correction for single-particle
12 electron microscopy *Ultramicroscopy* **106** 376-82
- 13 [87] Yan C, Hang J, Wan R, Huang M, Wong C C and Shi Y 2015 Structure of a yeast
14 spliceosome at 3.6-ångström resolution *Science (New York, N.Y)* **349** 1182-91
- 15 [88] Yan R, Edwards T J, Pankratz L M, Kuhn R J, Lanman J K, Liu J and Jiang W 2015
16 Simultaneous determination of sample thickness, tilt, and electron mean free path
17 using tomographic tilt images based on Beer-Lambert law *Journal of structural biology*
18 **192** 287-96
- 19 [89] Yoshioka C, Carragher B and Potter C S 2010 Cryomesh: a new substrate for cryo-
20 electron microscopy *Microsc Microanal* **16** 43-53
- 21 [90] Yu G, Li K and Jiang W 2016 Antibody-based affinity cryo-EM grid *Methods*
- 22 [91] Zewail A H 2010 Four-dimensional electron microscopy *Science (New York, N.Y)* **328**
23 187-93
- 24 [92] Zhang K 2016 Gctf: Real-time CTF determination and correction *Journal of structural*
25 *biology* **193** 1-12
- 26 [93] Zhang K, Foster H E, Rondelet A, Lacey S E, Bahi-Buisson N, Bird A W and Carter A P
27 2017 Cryo-EM Reveals How Human Cytoplasmic Dynein Is Auto-inhibited and
28 Activated *Cell* **169** 1303-14 e18
- 29 [94] Zheng S Q, Palovcak E, Armache J P, Verba K A, Cheng Y and Agard D A 2017
30 MotionCor2: anisotropic correction of beam-induced motion for improved cryo-
31 electron microscopy *Nature methods* **14** 331-2

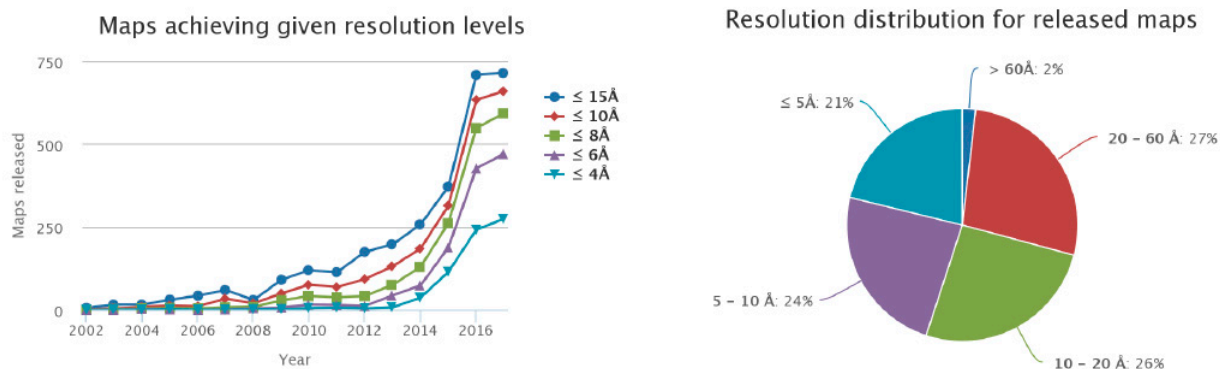
32

33

1

Figures

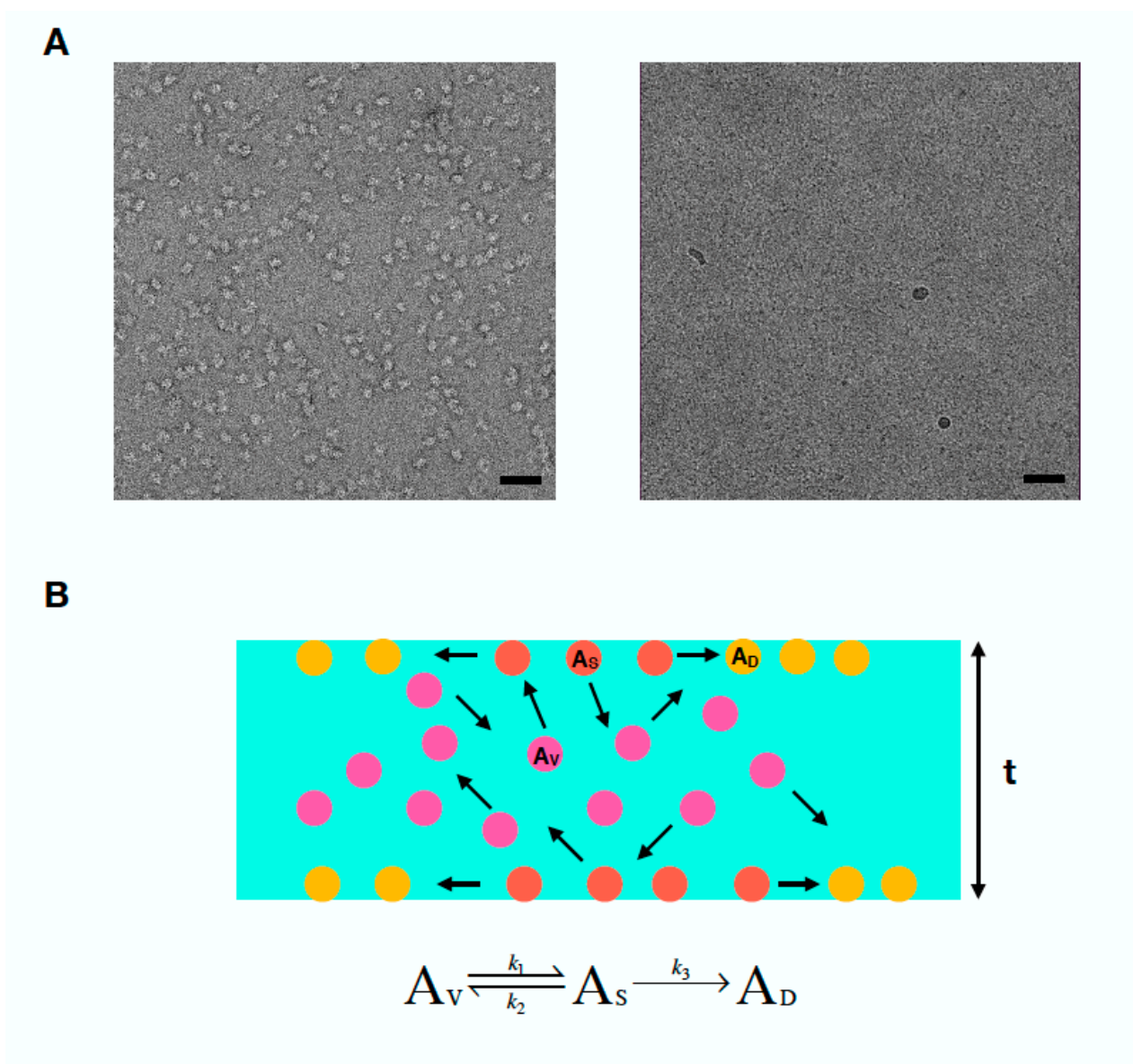
2



3

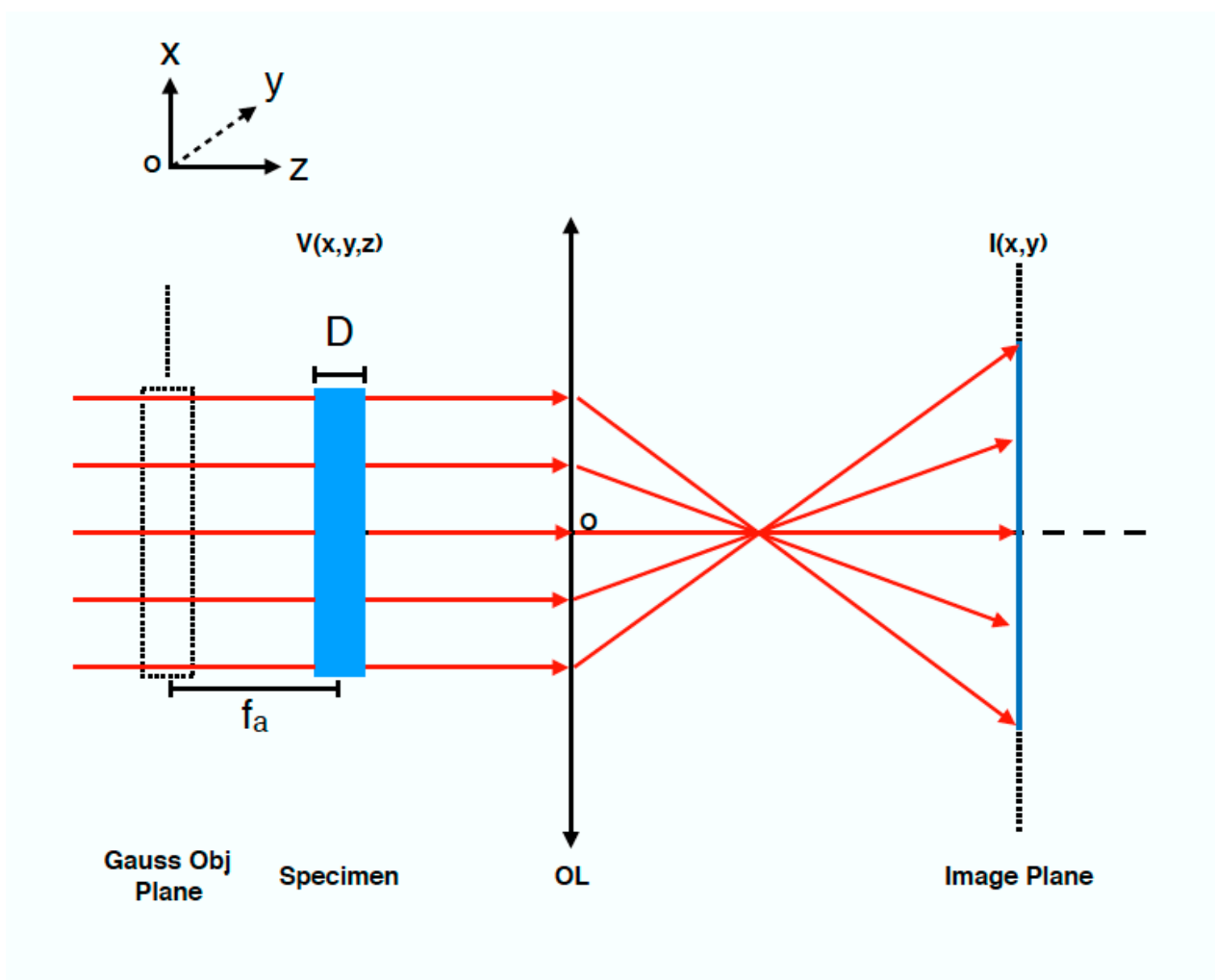
4 **Figure 1. Statistics of the electron density maps deposited in EMDB (Electron**
5 **Microscopy Data Bank).** The annual numbers of released maps with different reported
6 resolutions are plotted from 2002 to 2017 (left). And the distribution of all the released maps
7 till 2017 is statistically plotted vs different resolutions (right). Both panels were generated
8 using the tool of EMDB (<http://www.ebi.ac.uk/pdbe/emdb>).

9



1

2 **Figure 2. Air-water interface effects during specimen cryo-vitrification.** **A.** The bio-
 3 macromolecule specimen exhibits homogenous distribution and good shape in negative
 4 electron microscopy (left), but is prone to degrade and hard to observe in cryo-electron
 5 microscopy (right). Scale bar, 50 nm. **B.** A diagram showing the physical process during
 6 specimen cryo-vitrification. Bio-macromolecules in native state (A_V) are colored in pink,
 7 those (A_S) absorbed to air-water interface are colored in orange, and that (A_D) denatured
 8 in yellow. The thickness (t) of the solution layer after blotting is between 30 ~ 100 nm.



1

2 **Figure 3. A diagram showing the image formation of a think specimen with the**
 3 **averaged underfocus f_a .** Gauss Obj Plane, the plane where the idea objective locates
 4 according to Gauss image formation formula. D , the thickness of the specimen. OL,
 5 objective lens. $V(x,y,z)$, the density function of the specimen. $I(x,y)$, the image function at
 6 the image plane.